Calculating Percentage of PCNA- or TUNEL-positive Tumor or Ectopic Cells

After immunostaining tissue sections from three *SmoA1*;*Bmi1*$^{+/+}$ and three *SmoA1*;*Bmi1*$^{-/-}$ animals for PCNA or TUNEL as described in the Materials and Methods section, we photographed 10 random nonoverlapping high-power fields of tumor or ectopic tissue for each animal. If there were fewer than 10 high-power fields' worth of cells in a given *SmoA1*;*Bmi1*$^{-/-}$ lesion, we photographed all ectopic cells present in the section. We then counted both the number of PCNA or TUNEL-positive nuclei per field and the total number of nuclei per field, and divided the number of positive nuclei by the total number of nuclei to obtain the percent positive nuclei. *P* values were calculated using the 2-tailed *t* test, assuming unequal variances.

Quantitative Real-time RT-PCR Primer Sets

Quantitative polymerase chain reaction was performed as described in the Materials and Methods section, using the following primer sets:

Actin: 5′-tgttaccaactgggacgaca-3′ and 5′-tctcagctgtggtggtgaag-3′.
Math1: 5′-tgcgctcactcacaaataag-3′ and 5′-taacaacacaatagtccgtgttc-3′.
N-myc: 5′-gctgcggtcactagtgtgtc-3′ and 5′-ggagaagcctcgctcttgat-3′.
CyclinD1 [12]: 5′-ctctggctctgtgcctttct-3′ and 5′-ccggagactcagagcaaact-3′.
CyclinD2 [12]: 5′-ttcagcaggatgatgaagtga-3′ and 5′-gagaaggggctagcagatga-3′.

Supplementary References

[1] Oliver TG, Read TA, Kessler JD, Mehmeti A, Wells JF, Huynh TT, Lin SM, and Wechsler-Reya RJ (2005). Loss of patched and disruption of granule cell development in a pre-neoplastic stage of medulloblastoma. *Development* **132**, 2425–2439.

[2] Ueba T, Kadota E, Kano H, Yamashita K, and Kageyama N (2008). MATH-1 production by an adult medulloblastoma suggestive of a cerebellar external granule cell precursor origin. *J Clin Neurosci* **15**, 84–87.

[3] Hatton BA, Knoepfler PS, Kenney AM, Rowitch DH, de Alboran IM, Olson JM, and Eisenman RN (2006). N-*myc* is an essential downstream effector of Shh signaling during both normal and neoplastic cerebellar growth. *Cancer Res* **66**, 8655–8661.

[4] Pogoriler J, Millen K, Utset M, and Du W (2006). Loss of cyclin D1 impairs cerebellar development and suppresses medulloblastoma formation. *Development* **133**, 3929–3937.

[5] van der Lugt NM, Domen J, Linders K, van Roon M, Robanus-Maandag E, te Riele H, van der Valk M, Deschamps J, Sofroniew M, and van Lohuizen M (1994). Posterior transformation, neurological abnormalities, and severe hematopoietic defects in mice with a targeted deletion of the *bmi-1* proto-oncogene. *Genes Dev* **8**, 757–769.

[6] Marino S, Vooijs M, van Der Gulden H, Jonkers J, and Berns A (2000). Induction of medulloblastomas in p53-null mutant mice by somatic inactivation of Rb in the external granular layer cells of the cerebellum. *Genes Dev* **14**, 994–1004.

[7] Wang J, Lin W, Popko B, and Campbell IL (2004). Inducible production of interferon-gamma in the developing brain causes cerebellar dysplasia with activation of the Sonic hedgehog pathway. *Mol Cell Neurosci* **27**, 489–496.

[8] Lin W, Kemper A, McCarthy KD, Pytel P, Wang JP, Campbell IL, Utset MF, and Popko B (2004). Interferon-gamma induced medulloblastoma in the developing cerebellum. *J Neurosci* **24**, 10074–10083.

[9] Molofsky AV, He S, Bydon M, Morrison SJ, and Pardal R (2005). Bmi-1 promotes neural stem cell self-renewal and neural development but not mouse growth and survival by repressing the p16^{Ink4a} and p19^{Arf} senescence pathways. *Genes Dev* **19**, 1432–1437.

[10] Diamond I, Owolabi T, Marco M, Lam C, and Glick A (2000). Conditional gene expression in the epidermis of transgenic mice using the tetracycline-regulated transactivators tTA and rTA linked to the keratin 5 promoter. *J Invest Dermatol* **115**, 788–794.

[11] Grachtchouk V, Grachtchouk M, Lowe L, Johnson T, Wei L, Wang A, de Sauvage F, and Dlugosz AA (2003). The magnitude of hedgehog signaling activity defines skin tumor phenotype. *EMBO J* **22**, 2741–2751.

[12] Berman DM, Karhadkar SS, Hallahan AR, Pritchard JI, Eberhart CG, Watkins DN, Chen JK, Cooper MK, Taipale J, Olson JM, et al. (2002). Medulloblastoma growth inhibition by hedgehog pathway blockade. *Science* **297**, 1559–1561.

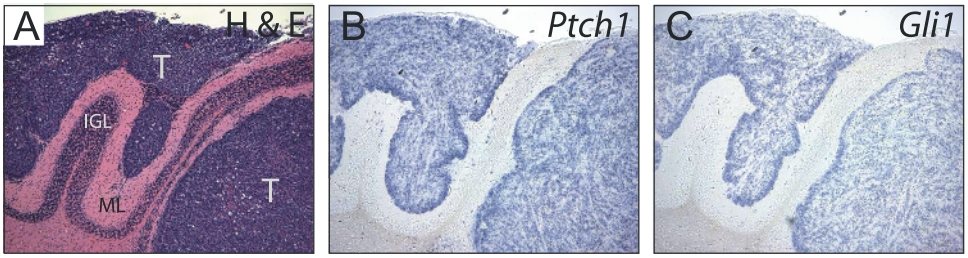

Figure W1. The Hh pathway is activated in SmoA1-induced medulloblastomas. (A) Hematoxylin and eosin staining of the cerebellum from a 7-week-old *SmoA1* mouse, demonstrating large tumor burden (T) outside the molecular layer (ML) and internal granular layer (IGL). (B–C) *In situ* hybridization for *Ptch1* (B) and *Gli1* (C) in nearby sections, demonstrating robust activation of the Hh pathway in tumors.

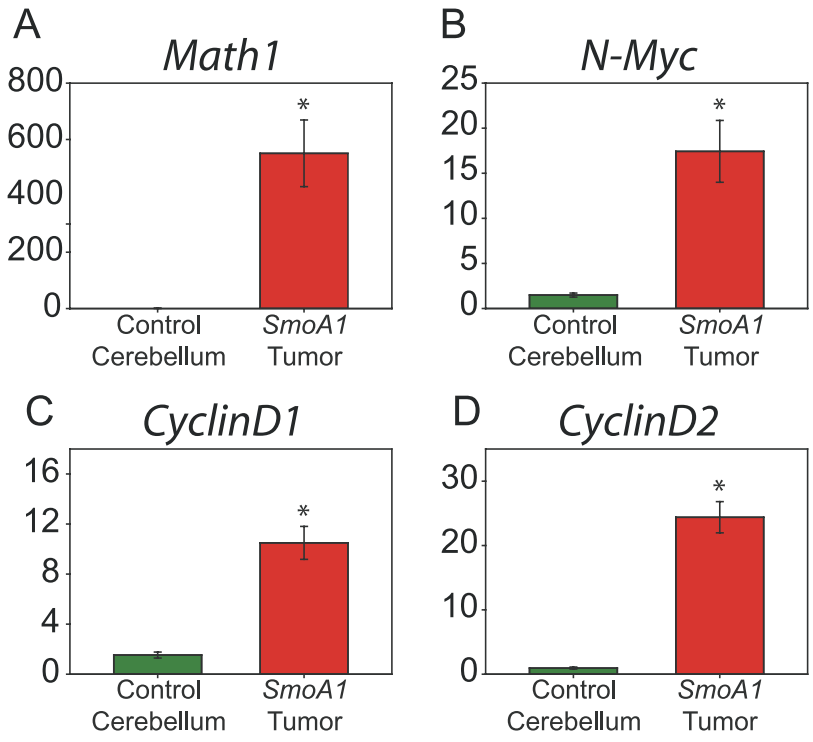

Figure W2. Medulloblastoma markers and Hh target genes are overexpressed in medulloblastomas. (A–D) Quantitative real-time RT-PCR reveals overexpression of *Math1* (A; 550-fold overexpression, $P = .0097$), *N-Myc* (B; 17-fold overexpression, $P = .012$), *CyclinD1* (C; 11-fold overexpression, $P = .0026$), and *CyclinD2* (D; 24-fold overexpression, $P = .00064$) in tumor-bearing cerebellum compared to control wild type cerebellum. $N = 5$ for each group; error bars indicate standard error of the mean; * indicates statistical significance.

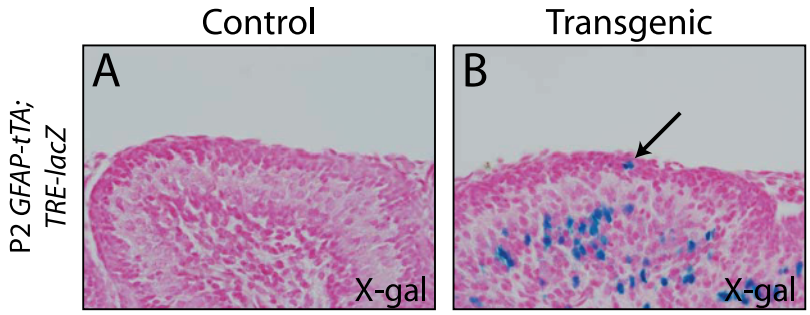

Figure W3. X-gal staining of 2-day-old *GFAP-tTA;TRE-lacZ* mouse cerebella. Overnight X-gal staining of P2 control (A) and *GFAP-tTA;TRE-lacZ* pups (B) revealed tTA activity in few cells scattered throughout the EGL at this stage. X-gal–stained cells in the EGL existed either singly or in small groups of cells.

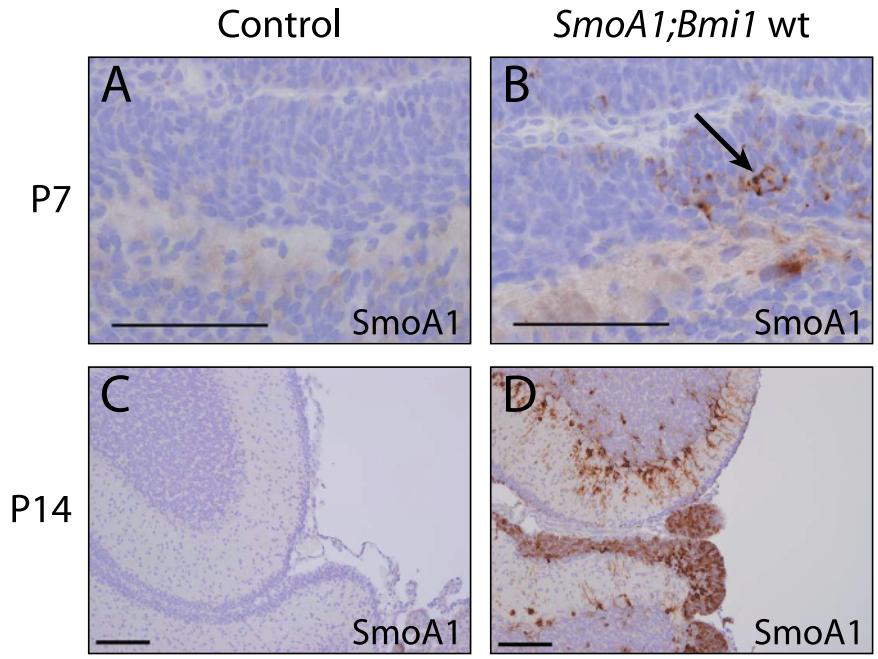

Figure W4. Immunostaining reveals focal SmoA1 expression in the mouse EGL at 7 and 14 days old. Detection of SmoA1 expression by immunostaining for the HA epitope tag revealed small clusters of SmoA1-positive cells in the EGL of 7-day-old pups (A, B, arrow), with only minor disruption of the normally smooth regular surface of the EGL. By 14 days old, whereas control EGL had begun to regress (C), readily identifiable SmoA1-expressing masses were already appreciable (D).

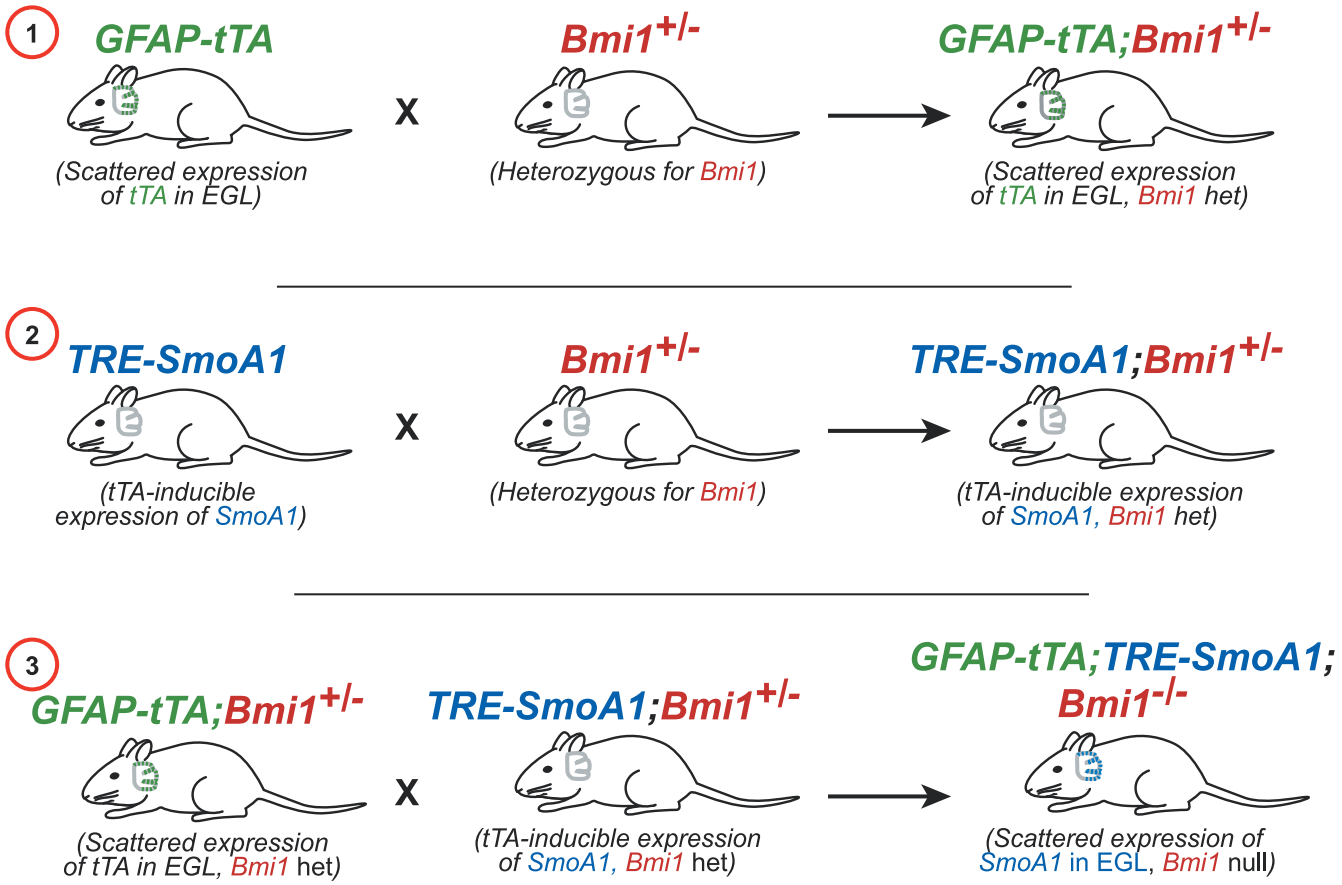

Figure W5. Three-step breeding scheme to generate *SmoA1;Bmi1*$^{-/-}$ mice. (1) *GFAP-tTA* and (2) *TRE-SmoA1* mice were independently crossed with *Bmi1*$^{+/-}$ mice to generate *GFAP-tTA;Bmi1*$^{+/-}$ and *TRE-SmoA1;Bmi1*$^{+/-}$ mice, respectively. These progeny were then intercrossed (3) to generate *GFAP-tTA;TRE-SmoA1;Bmi1*$^{-/-}$ mice, designated *SmoA1;Bmi1*$^{-/-}$. A predicted 1 of 16 newborn pups from the final crosses (*GFAP-tTA;Bmi1*$^{+/-}$ × *TRE-SmoA1;Bmi1*$^{+/-}$) express SmoA1 on a *Bmi1* null background (*GFAP-tTA;TRE-SmoA1;Bmi1*$^{-/-}$), but in reality, the actual proportion of mice obtained with this genotype is much lower because of the impaired viability of *Bmi1*$^{-/-}$ mice.

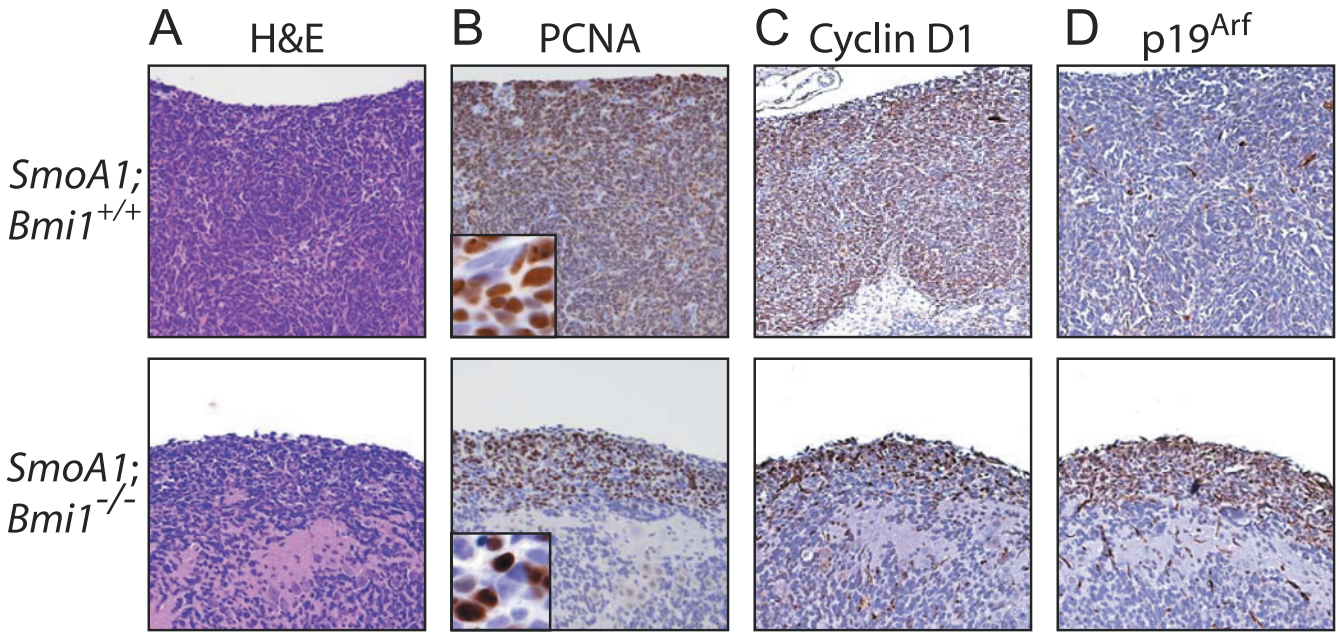

Figure W6. Cell cycle marker differences between intermediate tumor-like focus in P18 *SmoA1*;*Bmi1*$^{-/-}$ cerebellum and full-blown medulloblastoma in *SmoA1*;*Bmi1*$^{+/+}$ mice. (A) Hematoxylin and eosin staining of medulloblastoma *SmoA1*;*Bmi1*$^{+/+}$ and intermediate lesion (*SmoA1*;*Bmi1*$^{-/-}$). Histologic appearance of intermediate tumor-like lesion is similar to full-blown tumor, but the lesion is notably smaller. Shown in this image is the ectopic region with the maximal cross-sectional area. (B) PCNA stains both tumor and intermediate *Bmi1*$^{-/-}$ tumor-like focus, but stains fewer cells in the *Bmi1*-deficient lesion. Insets show higher magnification. Cyclin D1 expression is lower (C) and p19^{Arf} is elevated (D) in the *SmoA1*;*Bmi1*$^{-/-}$ lesion.

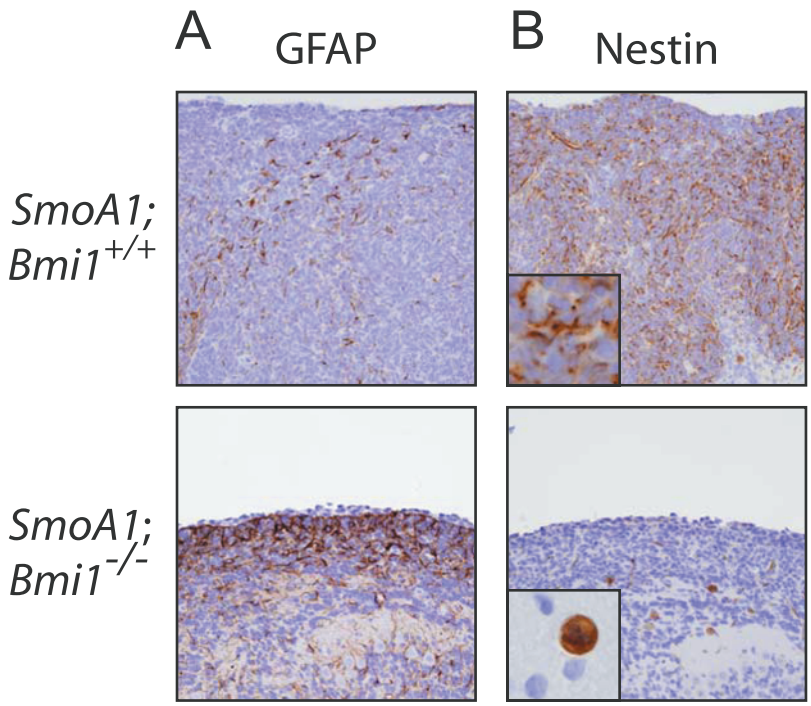

Figure W7. Increased glial density and loss of nestin expression in intermediate P18 *SmoA1*;*Bmi1*$^{-/-}$ tumor-like lesion. (A) Intense GFAP staining is seen in the outer region of the P18 *SmoA1*;*Bmi1*$^{-/-}$ tumor-like lesion, similar to the pattern seen in the ectopic regions of P21 animals. (B) Marked reduction of nestin-positive cells and alteration of subcellular nestin distribution is appreciable in *SmoA1*;*Bmi1*$^{-/-}$ mice at P18. Insets show higher magnification of tumor *SmoA1*;*Bmi1*$^{+/+}$ or molecular layer (*SmoA1*;*Bmi1*$^{-/-}$).